BIOLOGICAL CRYSTALLOGRAPHY

ISSN 1399-0047

Crystal structure and enzymatic properties of a broad substrate-specificity psychrophilic aminotransferase from the Antarctic soil bacterium *Psychrobacter* sp. B6

Anna Bujacz,* Maria Rutkiewicz-Krotewicz, Karolina Nowakowska-Sapota and Marianna Turkiewicz

Institute of Technical Biochemistry, Lodz University of Technology, Stefanowskiego 4/10, 90-924 Lodz, Poland. *Correspondence e-mail: anna.bujacz@p.lodz.pl

Received 19 November 2014
Accepted 23 December 2014

Keywords: aminotransferase; transaminase; substrate specificity; internal and external aldimine; psychrophilic enzyme.

PDB references: *Psy*ArAT, 4rkc; complex with aspartate, 4rkd

Supporting information: this article has supporting information at journals.iucr.org/d

Aminotransferases (ATs) are enzymes that are commonly used in the chemical and pharmaceutical industries for the synthesis of natural and non-natural amino acids by transamination reactions. Currently, the easily accessible enzymes from mesophilic organisms are most commonly used; however, for economical and ecological reasons the utilization of aminotransferases from psychrophiles would be more advantageous, as their optimum reaction temperature is usually significantly lower than for the mesophilic ATs. Here, gene isolation, protein expression, purification, enzymatic properties and structural studies are reported for the cold-active aromatic amino-acid aminotransferase (*Psy*ArAT) from *Psychrobacter* sp. B6, a psychrotrophic, Gram-negative strain from Antarctic soil. Preliminary computational analysis indicated dual functionality of the enzyme through the ability to utilize both aromatic amino acids and aspartate as substrates. This postulation was confirmed by enzymatic activity tests, which showed that it belonged to the class EC 2.6.1.57. The first crystal structures of a psychrophilic aromatic amino-acid aminotransferase have been determined at resolutions of 2.19 Å for the native enzyme (*Psy*ArAT) and 2.76 Å for its complex with aspartic acid (*Psy*ArAT/D). Both types of crystals grew in the monoclinic space group $P2_1$ under slightly different crystallization conditions. The *Psy*ArAT crystals contained a dimer (90 kDa) in the asymmetric unit, which corresponds to the active form of this enzyme, whereas the crystals of the *Psy*ArAT/D complex included four dimers showing different stages of the transamination reaction.

1. Introduction

Aminotransferases (ATs) belong to a vast group of pyridoxal 5′-phosphate (PLP)-dependent enzymes which constitute about 4% of all enzymes classified by the Enzyme Commission up to 2003. These enzymes include not only transferases, but also lyases, isomerases, a few oxidoreductases and hydrolases (Percudani & Peracchi, 2003). After glutamate and alanine dehydrogenases, and glutamate synthase, which convert inorganic nitrogen to amino groups, ATs are the most important catalytic proteins in ammonia metabolism. They primarily take part in distribution of amino groups in a range of different carbon skeletons, which is of crucial importance in the biosynthesis and degradation of various amino acids and other biomolecules (Hwang *et al.*, 2005). Some ATs, for example D-ATs from bacilli, participate in the metabolism of D-amino acids, which is indispensable for the synthesis of peptidoglycans and other secondary metabolites (Taylor *et al.*, 1998).

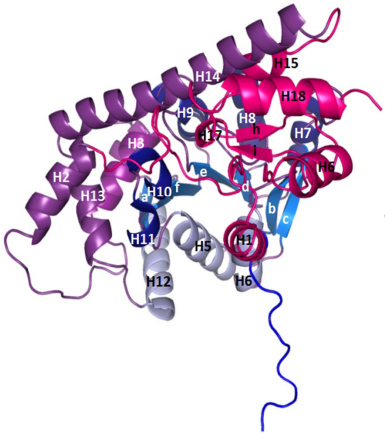

ATs, as enzymes that are mostly involved in central metabolism, are found in all domains of life (Archaea, Bacteria and Eukarya); they catalyze the transfer of an amino group from an amino acid to a 2-oxoacid in two similar half-reactions (Fig. 1). In the first half-reaction an α-amino acid and water react with a PLP–enzyme to form a homologous 2-oxoacid (product 1) and a pyridoxamine 5′-phosphate (PMP)–enzyme complex. In the second half-reaction a second 2-oxoacid reacts with the PMP–enzyme to yield the corresponding α-amino acid (product 2) and water. The catalytic mechanism of aminotransferases is defined as a ping-pong bi-bi mechanism. The transamination reaction is reversible, with its direction being determined by the excess of reactants (Kirsch *et al.*, 1984; McPhalen *et al.*, 1992).

In contrast to their extensive functional variety, PLP-dependent enzymes are characterized by relatively limited structural diversity. In 1995, on the basis of their fold, they were divided into five families (Grishin *et al.*, 1995), originally called 'classes'. It is currently known that this distribution also reflects an independent evolutionary path for each of the five protein families (Metha & Cristen, 2000; Jensen & Gu, 1996). All of the ATs (except for D-alanine aminotransferase) belong to family (or fold type) I, which is further divided into subfamilies α [aspartate aminotransferases (AspATs) and aromatic amino-acid aminotransferases (ArATs)] and β (AspATs) (Jensen & Gu, 1996). The sequence identities of the enzymes within each subfamily are at the level of above 30%, whereas the identities between the members of subfamilies Iα and Iβ are lower than 15% (Muratore *et al.*, 2013; Wu *et al.*, 2011; Peña-Soler *et al.*, 2014).

Enzymes are of special importance for potential industrial applications. They can be used as biocatalysts instead of chemical catalysts, thus leading to the production of high-quality products without harmful effects on the environment. The enzymes from extremophilic microorganisms are especially valuable. Such enzymes possess unique properties owing to the necessity of functioning in environments that are normally unfavourable for enzymatic catalysis. The ecological and economical aspects are necessary to consider when designing any production process. For this reason, the industry actively looks into the possibility of lowering the temperature at which processes must be conducted, as heating highly influences both the ecological and the economical properties of a production process. The most desirable are psychrophilic enzymes, which exhibit activity at a level comparable to their mesophilic homologues but at lower temperatures (Seetharamappa *et al.*, 2007; Fields, 2001). An additional advantage of the psychrophilic aromatic amino-acid aminotransferase from the Antarctic soil bacterium *Psychrobacter* sp. B6 (*Psy*ArAT) investigated here is the ability to catalyze the transamination reaction in an environment characterized by low water activity, as is typical for Antarctic soil (Struvay & Feller, 2012).

Since the ability of an enzyme to overcome the energetic barrier of reaction is based on modifications in tertiary structure, crystallographic studies are necessary to fully describe the protein, its mechanism of action and the molecular basis of its adaptation to specific environmental conditions. In the last decade, several ATs, among them the hyperthermophilic ArAT from *Pyrococcus horikoshii* (Matsui *et al.*, 2000) and the thermophilic AspAT from *Thermotoga maritima* (Schwarzenbacher *et al.*, 2004), have been characterized using crystallographic techniques. However, structural research on psychrophilic aminotransferases is less advanced. To date, only a model of a psychrophilic AspAT from *Pseudoalteromonas haloplanktis* TAC 125 has been constructed on the basis of sequence homology with other AspATs (Birolo *et al.*, 2000). Here, we present the first crystal structure of a psychrophilic aromatic amino-acid aminotransferase (*Psy*ArAT).

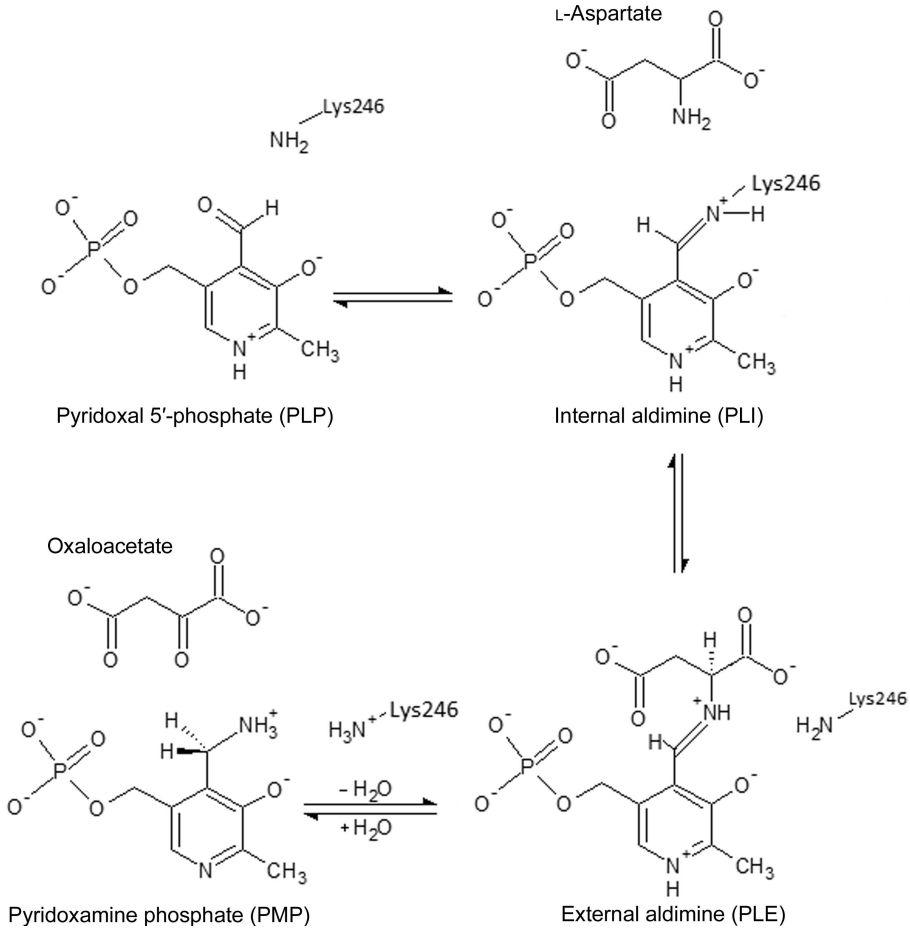

Figure 1
The mechanism of the transamination half-reaction catalyzed by *Psy*ArAT.

2. Materials and methods

2.1. Gene identification and sequencing

The psychrotrophic, Gram-negative coccobacillus *Psychrobacter* sp. B6 originated from the Antarctic microorganism collection owned by the Institute of Technical Biochemistry, TUL, Poland. This bacterium grows in the temperature range 0–30°C with an optimum at 20°C. Strain B6, isolated from a soil sample obtained from the coast of Admiralty Bay (close to the Henryk Arctowski Polish Antarctic Station, King George Island, Southern Shetlands, 62° 10′ S, 58° 28′ W), was identified based on the partial sequences of its 16S rRNA gene (Kaufman-Szymczyk *et al.*, 2009). An alignment of the B6 16S rRNA gene sequence (GenBank accession No. EF028072) with the sequences available in the GenBank/EMBL database was performed using *BLASTN* (Altschul *et al.*, 1990) and demonstrated that strain B6 is closest to *P. cryohalolentis* and *P. arcticus* (99% identity).

The aminotransferase gene (*psyarat*) was isolated from the chromosomal DNA of *Psychrobacter* sp. B6, which was obtained after cell lysis by lysozyme using a Genomic Mini kit (A&A Biotechnology, Poland; Kaufman-Szymczyk *et al.*, 2009). Specific primers for PCR amplification (AroTF, 5′-ATA TCT AGA ATG TTT GAA CGT ATC GAT TAC TAT GCC GGT GAC-3′; AroTR, 5′-ATA CTC GAG TTT ATC GTC GTC ATC GTC TTT TAA GAC GTC AAC CAT G-3′) were designed basing on the flanking regions of putative aromatic amino-acid aminotransferase gene sequences from *P. cryohalolentis* K5 and *P. arcticus* 273-4 (NCBI Genome Database accession Nos. NC_007969 and NC_007204, respectively). PCR was performed in a T-Personal thermocycler (Biometra) using *Taq* polymerase (Invitrogen, Frederick, Maryland, USA). The PCR conditions were as follows: denaturation at 94°C for 5 min followed by 30 cycles of amplification at 94°C for 1 min, 55°C for 1 min and 72°C for 1 min, followed by a final extension at 72°C for 5 min. The amplification product was analyzed by electrophoresis in 1.5% agarose gel stained with ethidium bromide and sequenced in the DNA Sequencing and Oligonucleotide Synthesis Laboratory, Institute of Biochemistry and Biophysics of the Polish Academy of Sciences, Warsaw.

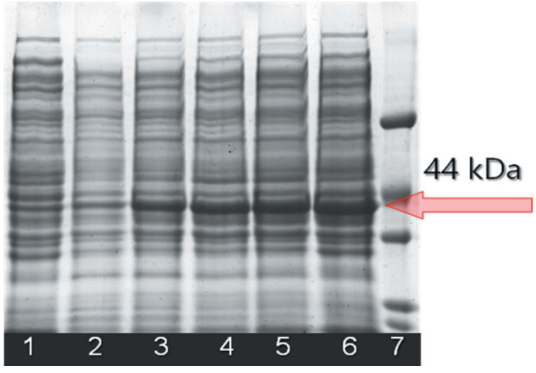

Figure 2
SDS–PAGE of cell-free extracts from recombinant *E. coli* BL21(DE3)-pLysS cells during induction of expression with IPTG. Lane 1, control *E. coli* BL21(DE3)pLysS cell lysate; lane 2, *E. coli* BL21pLysS/*psyAT* cell lysate before induction with IPTG; lanes 3, 4, 5 and 6, *E. coli* BL21(DE3)pLysS/*PsyAT* cell lysate 1, 3, 5 and 20 h after induction with IPTG, respectively; lane 7, protein molecular-mass markers (66, 45, 36, 29 and 24 kDa).

2.2. Protein expression and purification

The *psyarat* gene was cloned into pET303/CT-His expression vector (Invitrogen), which enables the addition of a histidine tag to the C-terminus of the recombinant protein, and the resulting recombinant vector p11 was used for the expression of aminotransferase in *Escherichia coli* strain BL21(DE3)pLysS under control of the T7 promoter. Culture of the transformed bacteria was carried out at 37°C in lysogeny broth (LB) liquid medium (1% Bacto Peptone, 0.5% yeast extract, 1% NaCl) supplemented with ampicillin (100 µg ml^{-1}; a selective marker of transformant cells containing p11 vector) and chloramphenicol (50 µg ml^{-1}; a selective marker of host strain enriched with pLysS plasmid). 100 m*M* isopropyl *β*-D-1-thiogalactopyranoside (IPTG) was added to induce recombinant protein production when the OD_{600} of the culture reached a level of between 0.5 and 0.6, and incubation was continued at 30°C. To optimize the efficiency of recombinant protein expression, 1 ml samples of the culture were collected at 1, 3, 5, 18 and 20 h and the level of expression of *Psy*ArAT was evaluated by SDS–PAGE of the transformed *E. coli* intracellular proteins (Fig. 2).

The fact that the enzyme was obtained with an oligohistidine tag at the C-terminus allowed a one-step purification procedure using affinity chromatography on a HisTrap HP nickel column (Amersham Bioscience, Corston, England). Cell-free protein extract was obtained by the sonication of *E. coli* cells in 0.02 *M* phosphate buffer pH 7.4 using a Bandelin Sonopuls GM 3200 (20 kHz, 25–150 W) with a KE76 probe twice for 2 min at 0°C and 30% amplitude with a pulse every 3 s with 1 s breaks. The samples were centrifuged for 20 min at 4°C (10 000 rev min^{-1}) and the supernatant was supplemented with 0.5 *M* NaCl and 0.02 *M* imidazole and introduced onto a HisTrap HP column previously equilibrated with the same buffer. The protein was eluted with 0.02 *M* phosphate buffer pH 7.4 containing 0.5 *M* NaCl and 0.5 *M* imidazole. The collected fractions were assayed for ArAT activity as a test of the protein content. The retained imidazole used for protein elution was removed by filtration with Amicon Ultra filters (30 kDa cutoff; Merck Millipore Corporation, Billerica, Massachusetts, USA). The protein solution was further desalted on a Sephadex G-15 column using a buffer consisting of 10 m*M* Tris–HCl pH 7.4. Purification of the recombinant protein was confirmed by SDS–PAGE analysis.

2.3. Enzymatic assays and other biochemical methods

The activity of ArAT was assayed by the spectrophotometric method based on the arsenate-catalyzed formation of aromatic 2-oxoacid-enol–borate complexes that show absorption maxima at 300, 310 and 330 nm for phenylpyruvate, *p*-hydroxyphenylpyruvate and indolepyruvate

Table 1
X-ray data-collection and crystal structure-refinement statistics.

Values in parentheses are for the last resolution shell.

	*Psy*ArAT (PDB entry 4rkc)	*Psy*ArAT/D (PDB entry 4rkd)
Data collection		
Radiation source	X13, DESY	BL14.1, BESSY
Wavelength (Å)	0.8020	0.9184
Temperature (K)	100	100
Space group	$P2_1$	$P2_1$
Unit-cell parameters (Å, °)	a = 74.69, b = 62.11, c = 85.89, β = 102.9	a = 92.25, b = 103.23, c = 165.78, β = 98.6
Resolution range (Å)	50.0–2.19 (2.27–2.19)	50.0–2.76 (2.86–2.76)
Reflections collected	197117	229747
Unique reflections	39647	77222
Completeness (%)	99.9 (99.3)	97.4 (98.6)
Multiplicity	5.0 (4.3)	3.0 (2.3)
$\langle I\rangle/\langle\sigma(I)\rangle$	16.7 (3.7)	7.7 (2.3)
$R_{\rm int}$†	0.091 (0.386)	0.126 (0.517)
Refinement		
No. of reflections in working/test set	37644/1989	73358/3862
$R/R_{\rm free}$‡ (%)	14.2/20.3	17.3/22.2
No. of atoms		
Protein	6243	24932
Solvent	770	817
Ligands	74	200
R.m.s. deviations from ideal		
Bond lengths (Å)	0.02	0.02
Bond angles (°)	1.97	2.04
$\langle B\rangle$ (Å^2)	25.1	39.8
Residues in Ramachandran plot (%)		
Most favoured regions	91.1	90.8
Allowed regions	8.6	8.9
Disallowed regions	0.3	0.3

† $R_{\rm int} = \sum_{hkl}\sum_i |I_i(hkl) - \langle I(hkl)\rangle|/\sum_{hkl}\sum_i I_i(hkl)$, where $I_i(hkl)$ is the intensity of the ith observation of reflection hkl. ‡ $R = \sum_{hkl}\big||F_{\rm obs}| - |F_{\rm calc}|\big|/\sum_{hkl}|F_{\rm obs}|$ for all reflections, where $F_{\rm obs}$ and $F_{\rm calc}$ are observed and calculated structure factors, respectively. $R_{\rm free}$ is calculated analogously for the test reflections, which were randomly selected and excluded from the refinement.

complexes, respectively (Lin *et al.*, 1958; Andreotti *et al.*, 1994). The reaction was carried out in 0.1 *M* phosphate buffer pH 7.4 containing 2-oxoglutarate (2-OG; final concentration 10 m*M*), an aromatic amino acid (L-Phe, L-Tyr or L-Trp; 10 m*M*), PLP (40 µ*M*) and the enzyme solution. After 10 min incubation at 37°C the reaction was stopped with ice-cold 20% trichloroacetic acid (TCA), centrifuged (13 000 rev min^{-1}, 5 min, 4°C) and 0.5 ml supernatant was mixed with 2 ml 1 *M* sodium arsenate–1 *M* boric acid buffer pH 6.5 and incubated at 25°C for 15 min. The absorbance of the sample was measured against a blank containing the same components except that enzyme solution and TCA were added simultaneously. To calculate the amount of oxoacid produced, molecular absorbance coefficients of 9150, 12 400 and 12 700 were used for phenylpyruvate, hydroxyphenylpyruvate and indolepyruvate, respectively. One unit (1 U) of ArAT activity is equivalent to the conversion of 1 µmol aromatic amino acid (L-Phe, L-Tyr or L-Trp) per minute to the corresponding 2-oxoacid under the standard conditions of the reaction.

The spectrophotometric method of Karmen was used in the assay of AspAT activity (Karmen *et al.*, 1955; Bradford, 1976). Oxaloacetate, which is the product of transamination of L-Asp and 2-OG, is reduced to L-malate using L-malate dehydrogenase (MDH; EC 1.1.1.37) and NADH. The reaction mixture consisted of 0.1 *M* phosphate buffer pH 7.4, 25 m*M* L-Asp, 10 m*M* 2-OG, 0.35 m*M* NADH, 1.5 U MDH and enzyme solution, which had previously been pre-incubated (10 min at 37°C) with 40 µ*M* PLP. It was incubated at 25°C and the absorbance was measured at 340 nm every 30 s. To calculate the AspAT activity, the molecular absorbance coefficient of NADH at 340 nm was taken to be 6220. One unit of AspAT activity is equivalent to the conversion of 1 µmol L-Asp per minute to oxaloacetate under the standard reaction conditions.

The protein was assayed with the Coomassie Protein Assay reagent (Sigma, USA; Laemmli, Beguin *et al.*, 1970). SDS–PAGE of proteins was carried out on slabs (100 × 55 mm) of 10% polyacrylamide gel (Laemmli, Mölbert *et al.*, 1970). The samples were denatured for 10 min at 100°C in the presence of 10% SDS and 0.5% β-mercaptoethanol. The gels were stained with Coomassie Brillant Blue R-250.

The effect of temperature on the activity of the purified recombinant *Psy*ArAT and the native enzyme present in the cell-free extract of *Psychrobacter* sp. B6 were determined under standard conditions at temperatures ranging from 0 to 80°C. A culture of *Psychrobacter* sp. B6 was grown for 6 d with shaking at 6°C in liquid LB medium without antibiotics. In order to obtain a cell-free extract, the wet biomass was sonicated in the same conditions as those used for the recombinant *E. coli* strain. The thermostability of *Psy*ArAT was tested by a 60 min incubation of the purified enzyme solution at temperatures in the range 0–70°C, followed by residual activity assays under standard conditions.

The molecular mass of recombinant *Psy*ArAT was determined using molecular sieving on a HiLoad 16/60 Superdex 200 pg column previously calibrated with protein molecular-mass standards (44–669 kDa).

The Michaelis constant ($K_{\rm m}$) and the maximum reaction velocity ($V_{\rm max}$) were determined for L-Phe (0.1–10 m*M*) from double-reciprocal Lineweaver–Burk plots. The $k_{\rm cat}$ value was calculated using a molecular mass of 44 kDa for the *Psy*ArAT subunit.

2.4. Protein crystallization, diffraction data collection and crystal structure determination

The protein was concentrated to approximately 9 mg ml^{-1} in 10 m*M* Tris–HCl buffer pH 7.5 using Vivaspin concentrators with 10 kDa cutoff (Sartorius, Germany). For screening of initial crystallization conditions, Crystal Screen, Index and PEG/Ion from Hampton Research (Aliso Viejo, California,

USA) were used. Crystals of *Psy*ArAT were obtained in 0.2 *M* magnesium nitrate, 20% PEG 3350 in HEPES buffer pH 7.5. Crystals of the *Psy*ArAT/D complex cocrystallized with a 20-fold molar excess of aspartic acid were grown in 0.2 *M* magnesium acetate, 20% PEG 3350 in Tris–HCl buffer pH 8.5. The hanging-drop vapour-diffusion method was used for all crystallizations.

X-ray diffraction data for *Psy*ArAT were collected on beamline X13 at the DESY synchrotron in Hamburg, whereas data for *Psy*ArAT/D were measured on beamline BL14.1 at BESSY in Berlin (Mueller *et al.*, 2012). The measurements were carried out under a stream of cold nitrogen (100 K), but different cryoprotection was applied to the two crystals. The crystal obtained in the presence of magnesium nitrate was soaked for a few seconds in a drop consisting of a 1:1 mixture of reservoir and PEG 400/glycerol, while for the crystal obtained in the presence of magnesium acetate no additional cryoprotection was needed (Bujacz *et al.*, 2010).

The collected diffraction images were indexed and integrated with *DENZO*. The intensity data for *Psy*ArAT were scaled with *SCALEPACK* in the *HKL*-2000 suite (Otwinowski & Minor, 1997), whereas the data for *Psy*ArAT/D were scaled with *XDS* (Kabsch, 2010). Both crystal forms belonged to space group $P2_1$, but were not isomorphous. The statistics of the diffraction data are presented in Table 1.

The crystal structure of *Psy*ArAT was solved by molecular replacement with *MOLREP* (Vagin & Teplyakov, 2010) using its closest homologue, tyrosine aminotransferase (TyrAT) from *E. coli* [PDB entry 3fsl; triple mutant (P181Q, R183G, A321K); V. N. Malashkevich, B. Ng & J. F. Kirsch, unpublished work]. The *Psy*ArAT/D structure was solved by molecular replacement with *MOLREP* using the *Psy*ArAT dimer as a starting model. The Matthews coefficients (Matthews, 1968) indicated the presence of two monomers in the asymmetric unit of *Psy*ArAT (V_M = 2.20 Å^3 Da^{-1}) and eight monomers in *Psy*ArAT/D (V_M = 2.21 Å^3 Da^{-1}).

The structures were refined with *REFMAC*5 (Murshudov *et al.*, 1997, 2011) from the *CCP*4 package (Winn *at al.*, 2011). TLS parameters were used for both data sets, and additional local NCS restraints were applied for the *Psy*ArAT/D structure. Rebuilding of the protein models was carried out with *Coot* (Emsley & Cowtan, 2004), and the structures were validated with *PROCHECK* (Laskowski *et al.*, 1993) and *MolProbity* (Chen *et al.*, 2010). A summary of data-collection and refinement statistics is presented in Table 1.

3. Results and discussion

3.1. Heterologous expression and substrate specificity of *Psy*ArAT

The isolated *psyarat* gene encoding the putative aromatic amino-acid aminotransferase from *Psychrobacter* sp. B6 consists of 1197 nucleotides with a sequence 87% identical to the sequences of homologous genes from *P. cryohalolentis* and *P. arcticus*, confirming the previously demonstrated very close relationship to the cold-loving B6 strain species (Kaufman-Szymczyk *et al.*, 2009). The enzyme encoded by the *psyarat* gene, produced as a fusion protein with a histidine tag at the C-terminus in *E. coli* strain BL21(DE3)pLysS, was transformed with a p11 vector. Expression was induced with 1 m*M* IPTG while decreasing the temperature of the culture of the transformed strain from 37 to 30°C, which significantly increased the efficiency of the biosynthesis of the enzyme. Production of *Psy*ArAT was most efficient 20 h after induction and no inhibition of the growth of the recombinant strain was observed under these conditions. The efficiency of overexpression was satisfactory, yielding about 35 mg of purified protein per litre of culture, accounting for approximately 7% the total protein in the cell-free extract. The activity obtained from of 25 h culture of the recombinant *E. coli* strain was approximately 25-fold higher than from a 6 d culture of the parental strain at 6°C, which is the optimal temperature for growth of the wild-type strain. The purification procedure was also satisfactory in its performance (70% of the total activity was in the purified protein fraction), with the purity of the isolated protein exceeding 90%. The molecular weight of the enzyme determined by electrophoresis under denaturating conditions was approximately 44 kDa (Fig. 2), consistent with the theoretical mass of the protein calculated on the basis of translation of the *psyarat* gene (44.156 kDa). The molecular weight of the native enzyme determined by size-exclusion chromatography was 90 kDa, indicating that *Psy*ArAT exists as a homodimer in the native state. The purified *Psy*ArAT preparation exhibited the highest specific activity in the transamination reaction of L-Tyr with 2-OG (68.7 U per milligram of protein in standard conditions at 37°C and pH 7.4). The activity was almost identical when L-Phe and L-Trp were utilized as donors of the α-amino group but was lower than the activity with tyrosine (39.7 and 38.2 U per milligram of protein, respectively). The purified protein also exhibited aspartate aminotransferase activity (12.7 U per milligram of protein), although this activity was significantly lower than for the aromatic amino acids (Table 2).

Table 2
Specific activity (U per milligram of protein) of recombinant *Psy*ArAT.

Substrate	Tyr	Phe	Trp	Asp
Specific activity	68.7	39.7	38.2	12.7

These results indicated dual specificity of *Psy*ArAT (acceptance of aromatic and acidic amino acids as amino-group donors), which is characteristic of some aromatic amino-acid transaminases belonging to subfamily Iα (Hayashi *et al.*, 1993). It should be noted that aminotransferases with broader specificity are considered to be particularly attractive tools in the synthesis of L- and D-amino acids and their derivatives, which are used in the pharmaceutical industry for the synthesis of peptidomimetics and chiral building blocks (Okamoto *et al.*, 1998).

For standard activity assays, L-Phe was used as the amino-group donor at 25°C and pH 7.4. The Michaelis constant (K_m) for *Psy*ArAT is relatively low at 4.22 × 10^{-3} *M*, the maximum reaction rate (V_{max}), expressed as the specific activity, is 51.3 U

per milligram of protein, the catalytic constant (k_{cat}) is 38.5 s^{-1} and the catalytic efficiency constant (k_{cat}/K_m) is 9123 M^{-1} s^{-1}.

3.2. Psychrophilic properties

Studies of the thermal activity show that native (as present in cell-free extracts from *Psychrobacter* sp. B6) and recombinant *Psy*ArAT exhibit the same surprisingly wide activity range, since the enzyme is able to catalyze the transamination reaction at temperatures from 0 to 80°C, with the highest activity at 55°C (Fig. 3). Cold-adapted extracellular enzymes are usually characterized by lower thermal optima in the range 30–45°C. Although the thermal optimum of *Psy*ArAT is surprisingly high, it is still lower by 20°C than the thermal optimum of the homologous mesophilic ArAT from *E. coli*. For comparison, the thermal optimum of the only other characterized psychrophilic AT, AspAT from the Antarctic bacterium *P. haloplanktis*, is also relatively high and is only 11°C lower than that of the mesophilic analogue *E. coli* AspAT (Birolo *et al.*, 2000). Numerous studies have shown that in the case of some endocellular enzymes adaptation to low temperature may be limited to a lowered thermostability, with no significant rise in enzyme effectiveness under low-temperature conditions (Struvay & Feller, 2012). Indeed, the thermal stability assays prove that *Psy*ArAT completely preserves its functionality after 1 h incubation at a temperature of up to 30°C. A 60 min incubation at 40°C decreases the activity of the enzyme by only 10%, and total inactivation of the enzyme occurs after 1 h incubation at 60°C. These results suggest that the preferred temperature optimum range *in vitro*, where the activity of the enzyme is maintained, ranges from 15 to 30°C, as at higher temperature the enzyme is inactivated despite significantly higher activity. Nonetheless, *Psy*ArAT is able to effectively catalyze the transamination reaction in the temperature range 0–15°C.

To explain the phenomenon of cold adaptation of *Psy*ArAT, its sequence and three-dimensional structure were compared with those of mesophilic ArATs and AspAT. Features such as a decrease in the arginine:lysine ratio and an increase in the number of glycines and charged residues in *Psy*ArAT enable the enzyme to overcome the problem of the activation-energy barrier at low temperatures (Gianese *et al.*, 2001). The sequence analysis showed that the total content of polar amino acids in *Psy*ArAT is increased by 4.9% with respect to *E. coli* TyrAT, by 5.1% compared with *P. horikoshii* OT3 and by 5.2% compared with *Burkholderia pseudomallei* ArAT, with a total content of 49.1%. This increase is especially evident in the case of Asp content, with an increase of 3.3% (8.3% in *Psy*ArAT but only around 5% in mesophilic ATs), and Lys content, with an increase of 1.3% (4.6% in *Psy*ArAT and around 3.3% in mesophilic ATs). The Gly content in *Psy*ArAT (8.5%) is increased by 0.7–1% in comparison to TyrAT from *E. coli* and by 0.2% compared with ArAT from *B. pseudomallei*. For mesophilic ATs the ratio of Arg to Lys residues ranges between 1.57 and 2.03, whereas in the case of *Psy*ArAT it is only 0.95 owing to the decrease in the number of Arg residues and the increase in the number of Lys residues in the psychrophilic enzyme.

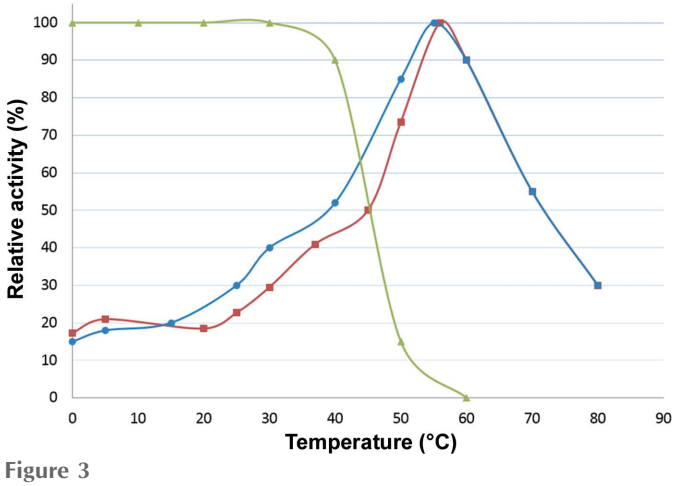

Figure 3
The effect of temperature on activity. Red squares, native enzyme in the cell-free extract from *Psychrobacter* sp. B6. Blue circles, recombinant enzyme. Green triangles, stability of *Psy*ArAT.

Another factor described by many authors which is responsible for cold adaptation and is connected to the secondary structure of the protein is an increased length of the loops (Ko *et al.*, 1999; Ura *et al.*, 2001; Jäger *et al.*, 1994). Recently, it was stated that extended length of the loops is not a necessity for psychrophilic enzymes (Peña-Soler *et al.*, 2014). The presented *Psy*ArAT does not have longer loops; on the contrary, it possesses an even more compact overall shape than its mesophilic and thermophilic analogues. The required flexibility of the regions involved in the enzymatic reaction is provided by introducing conformationally labile residues into the hinge regions. The presence of glycines in special locations, often in clusters of two (Feller, 2013), plays an important role in increasing the flexibility of the main peptide chain of *Psy*ArAT. Glycines are usually situated in the loops surrounding the active site of the enzyme and at the top of the loops where small and large domains interact. They are also located in the hinge region responsible for the swinging motion of the small domain that leads to the open and closed conformations of the enzyme. 13 glycines of the 33 present in the investigated *Psy*ArAT are characteristic of the described psychrophilic aminotransferase. The other 20 are predominantly conserved among the compared bacterial ArATs (Fig. 4*c*). The additional glycines Gly73, Gly155 and Gly291 located in the vicinity of the conserve glycines influence the flexibility of the already elastic peptide fragments. The others, Gly10, Gly15, Gly77, Gly131, Gly139, Gly145, Gly257, Gly273, Gly309 and Gly335, create additional flexible regions and not all of them are situated on loops or hinge regions; three of them, Gly77, Gly273 and Gly309, are present in the middle of α-helices.

3.3. Architecture of *Psy*ArAT

The arrangement of the secondary-structure elements among the aminotransferases in subgroup Iα is highly conserved, with an alteration in the number and the length of

small β-strand fragments. The monomer of *Psy*ArAT consists of two domains: the small N-C domain and the large cofactor-binding domain. Additionally, the enzyme possesses a long N-terminal arm through which the two monomers are anchored to each other (Fig. 5*a*), creating a functional dimer with a longest dimension of ∼100 Å.

The small domain, with a mostly helical architecture, is formed by residues from the N- and C-termini. The N-terminal part of this domain includes Met1–Leu66, whereas the C-terminal part extends from Pro286 to the end of the chain at Asp398. The N-terminal part of this domain contains two helices and a few loops. Ten residues creating random coil at the N-terminus interact with the surface of a neighbouring monomer in the area of the α-helix consisting of Val265–Tyr283. The C-terminal part of this domain is formed by five helical fragments and contains only two short strands of antiparallel β-sheet. The dominating element is a long nine-turn α-helix consisting of residues Ala301–Lys332. A parallel β-sheet is created between Lys28–Leu31 and Gly366–Met369 from the N- and C-terminal fragments, respectively (Figs. 4*a* and 4*b*).

The large domain has a mixed α–β–α architecture; its central part is created by a seven-stranded β-sheet. The strands are mostly parallel, with only one β-strand antiparallel to the others. The β-sheet is wrapped around three helices and its convex site is surrounded by four α-helices. The

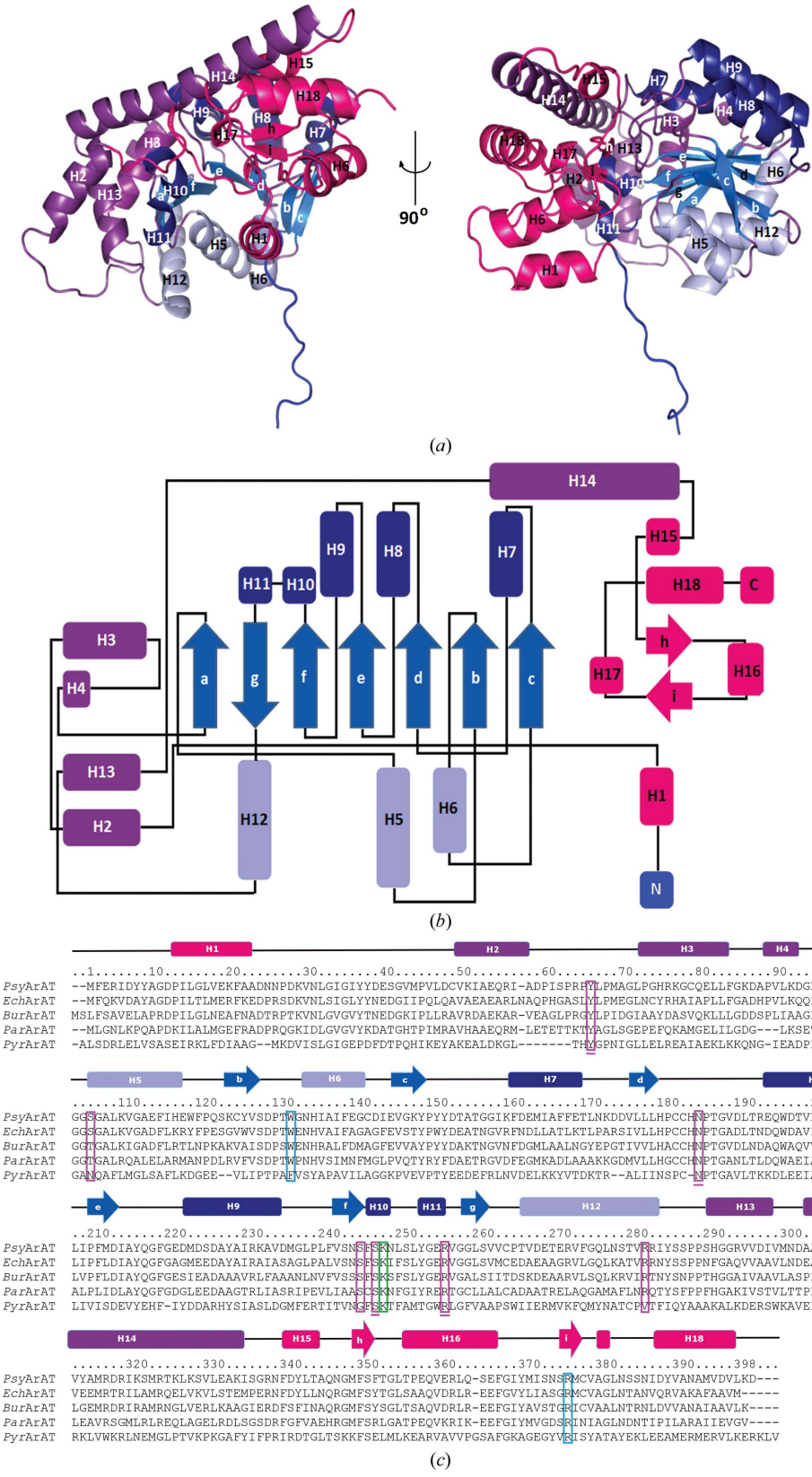

(*a*) (*b*) (*c*)

Figure 4
The arrangement of the *Psy*ArAT monomer with the secondary-structure elements coloured according to their distribution in the large and small domains. (*a*) Ribbon scheme. (*b*) Topology diagram. (*c*) Sequence alignment of *Psy*ArAT (numbering refers to *Psy*ArAT) with bacterial ArATs from *E. coli* (*Ech*ArAT; 57% similarity), *B. pseudomallei* (*Bur*ArAT; 48% similarity), *P. denitrificans* (*Par*ArAT; 37% similarity) and *P. horikoshii* OT3 (*Pyr*ArAT; 29% similarity). The lysine residue covalently bound to PLP is marked by a green frame. The amino acids interacting with PLP/PMP are marked by pink frames, residues involved in the interactions with PLE are underlined and the residues interacting with OAA are in blue frames. The cylinders and the arrows above the sequences and in the topology diagram represent helices and β-strands, respectively.

small domain is located over the large domain from the side of the edge of the β-sheet.

The monomer of *Psy*ArAT is composed of 18 helices (a total of 203 amino acids) and nine β-strands (a total of 44 amino acids), of which the small domain contains five helices (H1, H15, H16, H17 and H18; a total of 41 amino acids) and two short fragments of β-strand (h and i: a total of six amino acids), while the other 13 helices (162 amino acids) and seven β-strand fragments (38 amino acids) form parts of the large domain. The N-terminal arm of *Psy*ArAT is formed of random coil.

The dimer of *Psy*ArAT is an active form of the enzyme (Fig. 5*b*) and has an extended interface surface of 3215 Å^2. The buried surface of the dimer is large and represents 18% of the total monomer surface. The interactions between monomers in this dimer have a mostly hydrophobic character and cover three helices from the cofactor-binding domain and two helices from the small domain.

Four dimers of *Psy*ArAT/D create two tetramers in the asymmetric unit of the crystal (Fig. 5*c*). Different interactions are observed between the dimers belonging to these tetramers. In the *ABCD* tetramer the buried surface between the dimers is 958 Å^2, whereas in the *EFGH* tetramer the buried surface is much smaller (only 192 Å^2). The relatively small areas of contact between the dimers belonging to both tetramers suggest that tetramer formation is caused by crystal packing and is not physiologically relevant. The buried surface in each dimer in both tetramers in the *Psy*ArAT/D complex varies from 3271 to 3380 Å^2.

The magnesium cation present in both crystallization solutions, derived from magnesium nitrate in *Psy*ArAT and from magnesium acetate in *Psy*ArAT/D, is bound at the dimer-interface region of both structures discussed here. This ion is located on a noncrystallographic twofold axis and is surrounded by equivalent residues from two monomers. It is octahedrally coordinated by six water molecules (Fig. 6) which additionally interact with the same residues from the neighbouring monomers, including the side chains of Glu112 and Asp141, as well as the main-chain carbonyl O atoms of Gly139 and Cys140. The environment of the magnesium cation is very well defined by the electron-density map, especially in the structure of *Psy*ArAT (2.19 Å). The distances between the magnesium ions and the coordinated water molecules vary from 2.13 to 2.16 Å and are consistent with those described in the literature (Harding, 2006; Dokmanić *et al.*, 2008; Zheng *et al.*, 2014). Magnesium cations are present at the same location

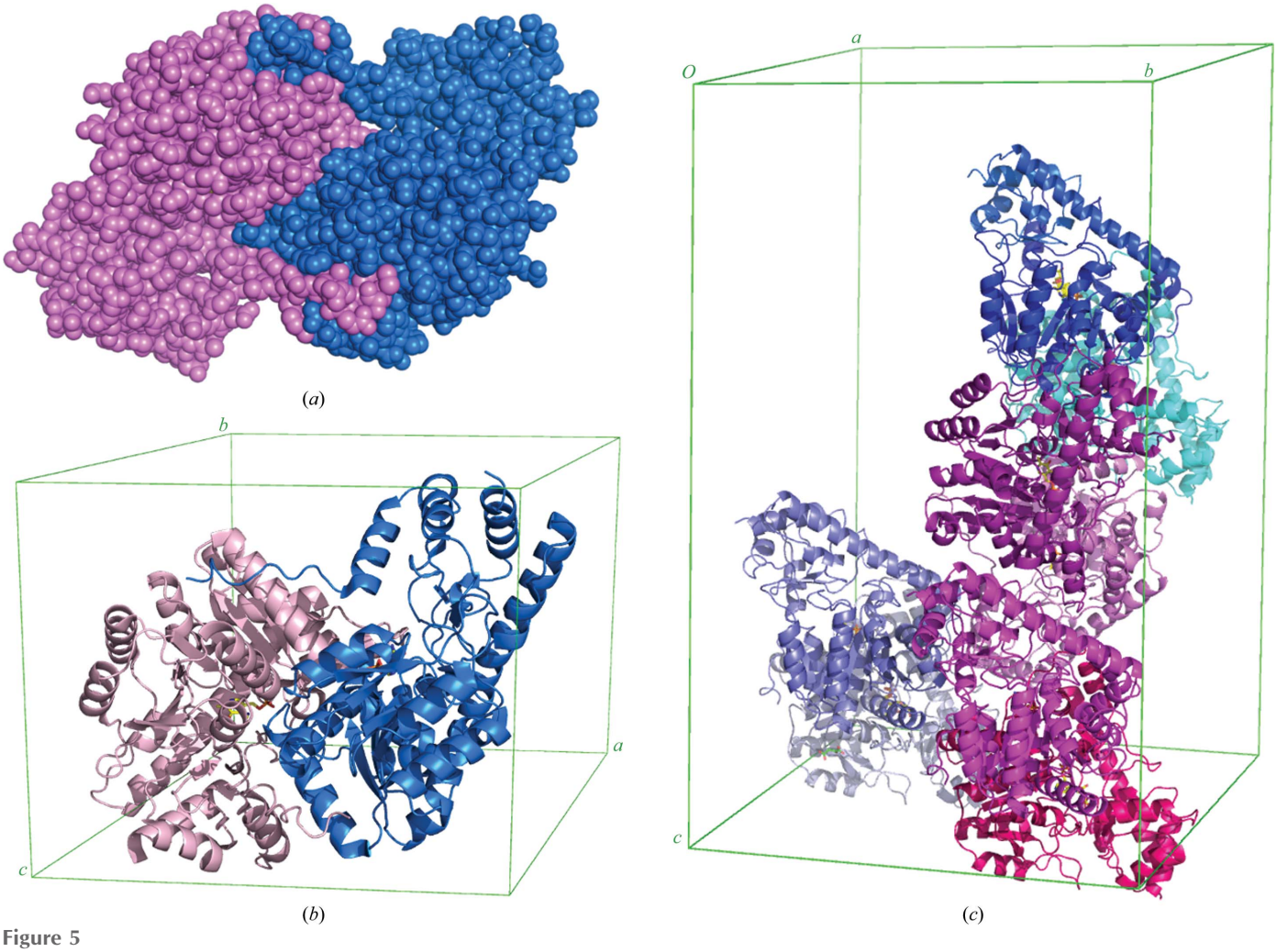

Figure 5
The interface of the functional *Psy*ArAT dimer (*a*), its packing diagram (*b*) and the arrangement of the *Psy*ArAT/D complex in the unit cell (*c*).

in all four dimers of *Psy*ArAT/D, but in two dimers one water molecule is not visible in the octahedral coordination sphere, probably owing to the lower resolution of this structure (2.76 Å) or/and just because of weaker interactions of this external water.

3.4. Active site

The active site of the enzyme is located at the top of the cofactor-binding domain. Two walls of the binding pocket are created by residues belonging to the small domain, Asp11–Leu14, Gly32–Gly34, Phe348 and Arg374, as well as by the loops from the second monomer, Arg63*–Met68* and Arg281*–Ser285*, bridging the small and large domains in the adjacent monomer.

The availability of the structure of *Psy*ArAT/D creates a unique opportunity to analyze the subsequent steps of the reaction catalyzed by this enzyme. Previously, this has been performed by comparisons of two or more structures obtained by crystallization with substrates and inhibitors (Miyahara *et al.*, 1994). The presence of L-aspartic acid, one of the substrates, in the crystallization buffer initiates a transamination reaction. The absence of the next keto-substrate prevents the shift of the equilibrium of transamination to terminate the reaction and various intermediate stages can be observed in the active sites of each monomer in this structure.

The PLP/PMP ligand, which was built in the enzyme by the bacteria and remains in the active centre even after the purification protocol, is kept in place by number of polar interactions and a hydrophobic contact with Trp130. Generally, the active site in all transition states looks very similar.

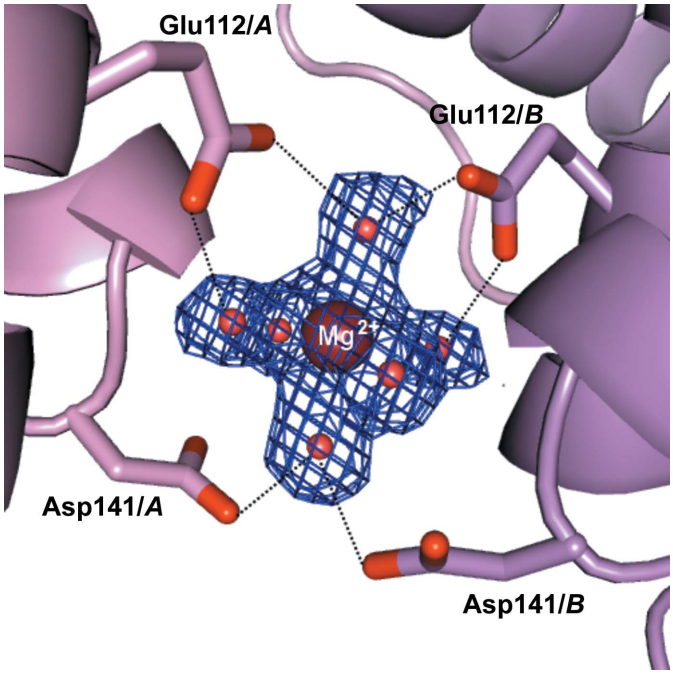

Figure 6
The magnesium ion bound at the dimer interface of *Psy*ArAT. The octahedral coordination sphere of Mg with six water molecules is visible in the $2F_o - F_c$ electron-density map contoured at the 1σ level.

However, we are able to see small changes in the conformation of the amino-acid side chains that are directly involved in PLP/PMP–protein interactions. In all stages three serines, Ser104, Ser243 and Ser245, as well as Arg254, create strong hydrogen bonds to the phosphate group of the cofactor (Fig. 7); Asn183 and Tyr214 interact with the hydroxyl group of the pyridine ring of PLP/PMP and Asp211 interacts with its N atom. The largest difference is visible in the distance between the hydroxyl group of Tyr65* (from an adjacent monomer) and the amine group of the catalytic Lys246. All of these interactions are captured at various stages of the catalytic reaction. Only the side chain of Lys246 changes its conformation depending on the stage of reaction. The PLP internal aldimine (PLI) is a state in which a covalent bond is formed between PLP and Lys246 (Fig. 7*b*); during the course of the transamination reaction this covalent bond is broken to form unbound PMP (Fig. 7*a*) in the active pocket and the amine group of the side chain of Lys246 creates a hydrogen bond to the carbonyl O atom of Gly34* from the adjacent monomer.

In the active pocket of monomer *G* the PLP external aldimine (PLE) is present (Fig. 7*c*) and a few additional polar contacts are made by the aspartic acid covalently bound to PLP; these are with Arg374, Trp130 and Tyr65*/*H* from the adjacent monomer.

In monomer *D* we observe the final stage of half-reaction, in which an oxaloacetate ion is present beside PMP. This released product of the half-reaction is kept in the active pocket by a number of polar contacts from two monomers (Fig. 7*d*). These include hydrogen bonds to Arg280*/*C*, Arg298*/*C*, Tyr65*/*C* and Trp130/*D* (2.75 Å) and a few polar contacts mediated by two water molecules with Arg374/*D*, Tyr214/*D* and Lys246/*D*.

3.4.1. Broad substrate specificity. Even though the active site of *Psy*ArAT is primarily designed to perform a transamination reaction with large aromatic amino acids as substrates, it has the ability to react with small acidic amino acids as well. This adaptability is based on the side-chain conformation of Arg280 belonging to the adjacent monomer, which creates the functional dimer, and Arg374 on the opposite site of the active-site pocket. Depending on their conformations, these two arginines may change the character of the active-site pocket from basic, capable of binding an acidic substrate, to more hydrophobic, suitable for the binding of aromatic amino acids. Additionally, the size and hydrophobicity of the active-site pocket can be modified by the conformation of the flexible loop Leu31–Ile35, which consists of two glycines and three hydrophobic residues.

3.5. Comparison of *Psy*ArAT/D monomers

Alignment of monomers based on a C^{α} superposition performed by the SSM function in *Coot* (Emsley & Cowtan, 2004) shows an r.m.s.d. between *Psy*ArAT/D monomers in the range 0.26–0.55 Å, which is surprisingly low when we take into consideration that these monomers exhibit different stages of the transamination reaction. The largest difference in r.m.s.d. is between monomers *D* and *G*, showing the end of the half-

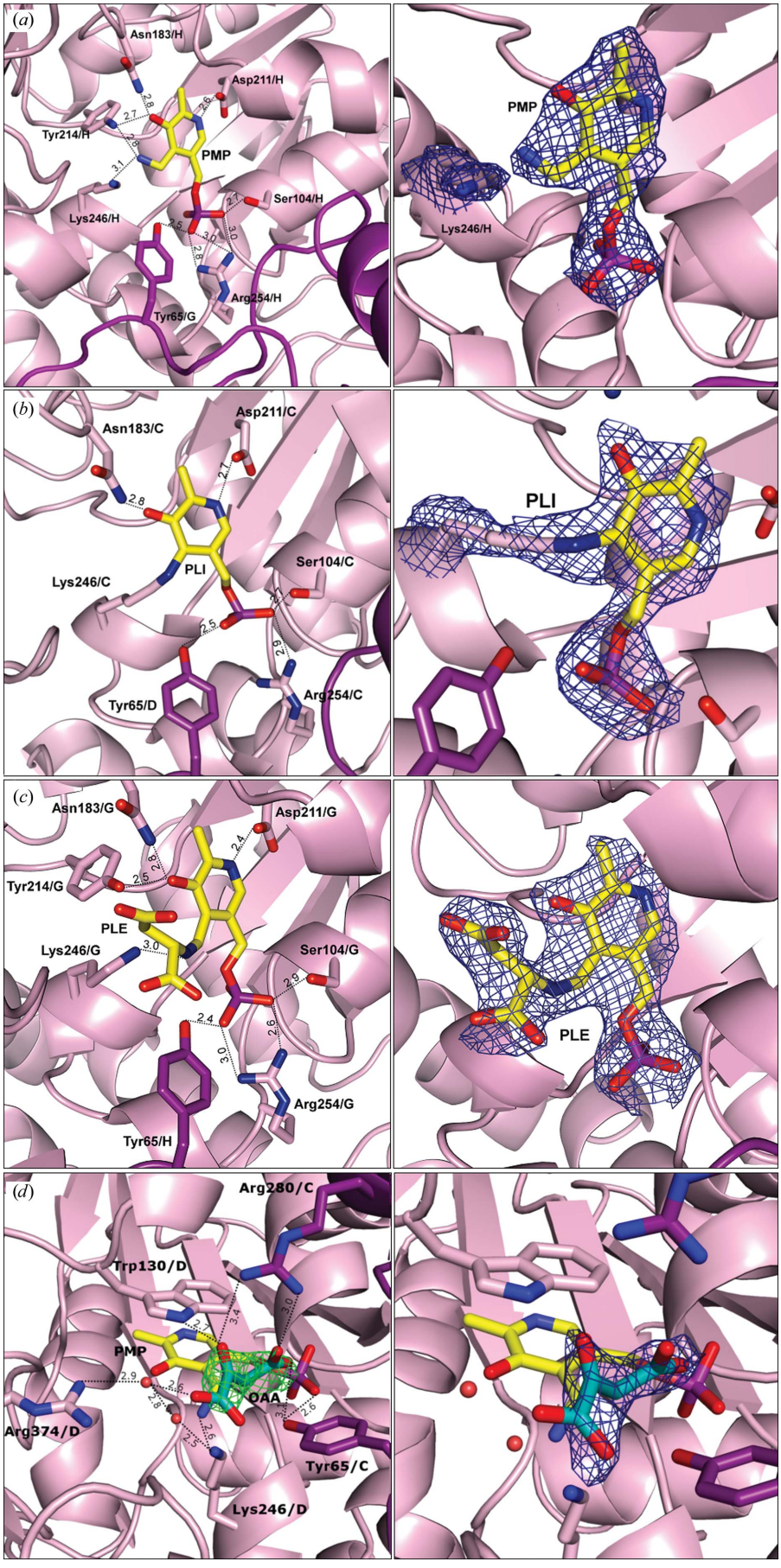

reaction and the external aldimine, the intermediate stage of transamination reaction, respectively. These results support the hypothesis that in bacterial aminotransferases the movement of the small domains associated with the closed and open conformations is much smaller than in eukaryotic aminotransferases (Ko *et al.*, 1999; Malashkevich *et al.*, 1993; Maity *et al.*, 2014).

In the *Psy*ArAT native structure the r.m.s.d. between the aligned monomers (*A* and *B*) is surprisingly high at 0.807 Å, which may be caused by two factors. One may be the fact that PMP is not bound to Lys246, and the other is connected to the different crystal contacts of each monomer in the crystal lattice. Both monomers in this dimer also differ from the monomers in the *Psy*ArAT/D complex, where monomer *A* exhibits an r.m.s.d. ranging from 0.32 to 0.50 Å when compared with all eight monomers and monomer *B* exhibits an r.m.s.d. ranging from 0.39 to 0.51 Å. The second factor seems to be more important, since we observed different conformations of the external loop Ile13–Lys28 and loop Ser327–Tyr340 as well as the C-terminus. Although the r.m.s.d. of the aligned monomers is generally quite low, the volume of the internal active-site pocket and the conformation of the side chains of the amino acids involved in PLP/PMP/product binding undergo noticeable changes. The largest of these are visible in the N-terminal fragment from Ile13 to Asn24, which in turn affects a significant number of contacts with the small domain. The conformation of the main chain in the active site is

Figure 7
The active pocket of *Psy*ArAT/D at four different stages of the transamination reaction. Interactions in the active pocket are shown on the left and $2F_o - F_c$ electron-density maps at the 1σ level on ligands are shown on the right. (*a*) The interactions of PMP with monomer *H*. (*b*) The interactions of the pyridoxal 5′-phosphate internal aldimine (PLI) in the active-site pocket of monomer *C*. (*c*) The interactions of the pyridoxal 5′-phosphate external aldimine (PLE) in monomer *G*. (*d*) The interactions of the released product of the half-reaction (oxaloacetate) and the $2F_o - F_c$ electron-density OMIT map at the 2.5σ level for the ligand (OAA), which was refined with 0.5 occupancy.

conserved in each monomer in both of the structures presented here.

3.6. Open and closed conformations

The transamination reaction can be performed only in a hydrophobic environment; therefore, conformational change of the structure of the enzyme is indispensable. This is obtained by a rotational movement of the small domain inwards and outwards relative to the active site. This movement of the small domain enables division of the enzyme structures into open and closed forms. The open form either enables the access of substrate or enables the release of product by moving the small domain outwards from the active site. The closed form provides the hydrophobic environment for the reaction after the substrate has already entered the active site by movement of the small domain towards the active site and by sealing the substrate at the active site from the solvent.

For a comparison of the closed and open forms of the enzyme we chose monomer *G* of *Psy*ArAT/D, in which an external aldimine (PLE) of PLP with bound aspartate is present in the active pocket, and monomer *C*, in which an internal aldimine (PLI) is present (PLP is covalently bound to Lys246). These two monomers superimposed with an r.m.s.d. of 0.53 Å. When the superposition was based on the large domains the r.m.s.d. was 0.36 Å. Although the r.m.s.d. value of the aligned monomers is low, the movement of the small domain is noticeable and the positions of the residues located at the top of this domain, close to the active site, differ by 1.3 Å.

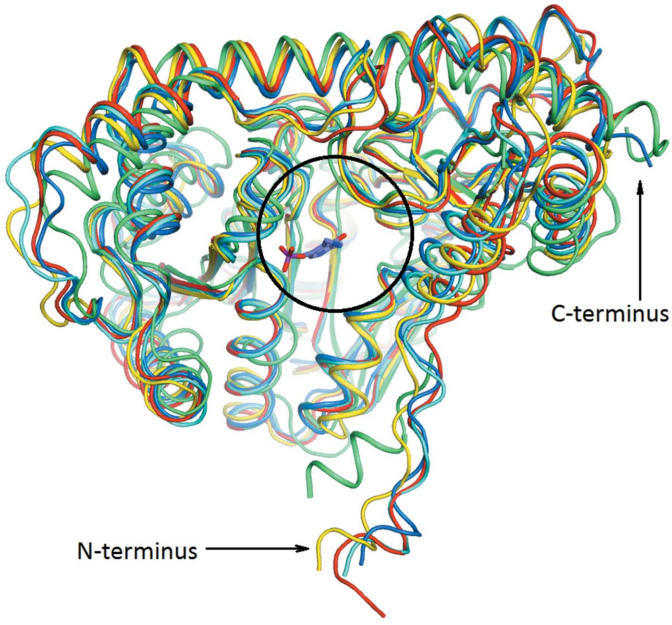

Figure 8
Superposed monomers of bacterial ArATs: *Psy*ArAT as investigated here (PDB entry 4rkc, blue), *Par*ArAT (PDB entry 1a4y, yellow), *Ech*ArAT (PDB entry 3fsl, cyan), *Bur*ArAT (PDB entry 4e4f, red) and *Pyr*ArAT (PDB entry 1dju, green). The circle shows the active centre with PLP.

Table 3
Results of *BLASTP* sequence alignment and r.m.s.d.s for the superposition in *Coot* of the *Psy*ArAT monomer with homologous mesophilic (PDB entries 3fsl from *E. coli*, 4f4e from *B. pseudomallei* and 1ay4 from *P. denitrificans*) and thermophilic (PDB entry 1dju from *P. horikoshii* OT3) bacterial ArATs.

	Identity (%)	R.m.s.d. (Å)
3fsl	57	0.93
4f4e	48	1.17
1ay4	37	1.59
1dju	29	2.23

Analysis of the structure of *Psy*ArAT showed that the movement accompanying the change in conformation was minimal for the main chains, but heavily impacted the conformation of the side chains of amino acids. Rotation of the side chain of Asp11 by almost 180° is the most significant difference, which leads to a change in the position of helix H1 and a reduction of the size of the entrance to the active site. Moreover, residues Ile13, Ile14 and Val17 create a hydrophobic plug that prevents solvent from entering the active site. Only a single water molecule, representing a side product of the reaction, was found in the active site of the closed form, while in the open form more water molecules were visible.

Analysis of the domain–domain interactions showed relatively small differences between the open and closed forms of the monomers, most likely resulting in only a small energy barrier between the two conformations. This situation is typical for the bacterial aminotransferases that were compared here, in which the open and closed conformations are more similar than in ATs of eukaryotes. The movement of the small domain in the open and closed conformations is more significant for the latter enzymes (McPhalen *et al.*, 1992; Malashkevich *et al.*, 1993; Maity *et al.*, 2014; Miyahara *et al.*, 1994).

3.7. Comparison of *Psy*ArAT with analogous bacterial ArATs

The AT structures available in the PDB belong to different classes and subgroups possessing various substrate specificities. Nevertheless, the aromatic aminotransferase from *Psychrobacter* sp. B6 (PDB entry 4rkc) presented here is the first structure of a psychrophilic bacterial ArAT.

The sequences of a large number of ArATs and AspATs available in the databases show similarity to the sequence of the psychrophilic AT investigated here. Many of them have quite high identity, from 57 to 37%, compared with *Psy*ArAT. For detailed structural comparisons we have chosen only bacterial aromatic amino-acid aminotransferases for which crystal structures are known. This narrowed our analysis to four other enzymes, three of which are mesophilic: tyrosine aminotransferase (TyrAT) from *E. coli* (PDB entry 3tat; *Ech*ArAT; Ko *et al.*, 1999) and the aromatic amino-acid aminotransferases from *Paracoccus denitrificans* (PDB entry 1ay4; *Par*ArAT; Okamoto *et al.*, 1998), *B. pseudomallei* (PDB entry 4f4e; *Bur*ArAT; Seattle Structural Genomics Center for Infectious Disease, unpublished work) and the thermophilic *Pyrococcus horikoshii* OT3 (PDB entry 1dju; *Pyr*ArAT;

Matsui *et al.*, 2000) (Table 3). All of the compared enzymes are represented in the PDB by a number of crystal structures, including mutants and complexes with ligands. Superposition of the crystal structure of *Psy*ArAT with the above bacterial aminotransferases shows extensive similarity in the overall structure, especially in the architecture of the catalytic centre (Fig. 8).

The goal of this analysis was to identify the structural features that are responsible for the temperature adaptation and substrate specificity of the investigated psychrophilic enzyme. Sequence alignment in *ClustalW* (Larkin *et al.*, 2007) showed the highest similarity (57%) to TyrAT (PDB entry 3tat; Ko *et al.*, 1999).

The catalytic Lys246 of *Psy*ArAT involved in PLP binding is conserved in all of the compared ATs. The other amino acids that take part in PLP or substrate/product stabilization are Tyr65, Ser104, Trp130, Asn183, Asp211, Tyr214, Ser243, Ser245, Arg254, Arg280 and Arg374, where the last two are only important for product binding (Fig. 4*c*).

The structure of *Psy*ArAT bears most similarity, both in sequence and in architecture, to those of aromatic aminotransferases, but it also exhibits significant similarity to AspATs from subgroup Iα, especially in the active-site region. It is important to note the differentiation between aminotransferases from subgroups Iα and Iβ, as subgroup Iα AspATs (for example, PDB entry 7aat; McPhalen *et al.*, 1992) are more similar to the ArATs (for example, PDB entry 3fsl; Ko *et al.*, 1999; 39.29% similarity), but subgroup Iβ AspATs (for example, PDB entry 1bjw; Nakai *et al.*, 1999) show lower similarity when aligned with ArATs (14.4% similarity to PDB entry 3fsl). The relatively high level of similarity of *Psy*ArAT to the AspATs from subgroup Iα (for example, 41.46% to PDB entry 7aat) may at least partially explain the double functionality of *Psy*ArAT.

3.7.1. Structural comparison of *Psy*ArAT with analogous ArATs from mesophilic bacteria. The structure of *Psy*ArAT displays the closest similarity to the mesophilic ArAT from *E. coli* (PDB entry 3tat; Ko *et al.*, 1999). For structural comparison the triple mutant of *E. coli* ArAT (PDB entry 3fsl) was used owing to better resolution and Ramachandran statistics (core r.m.s.d. of 0.93 Å; Table 3). Although the differences in the conformation of their main chains are minor, they can still be noticed (Fig. 8). The interactions between the large and small domains remain tighter: loop Ala57–Arg63 moves toward the second monomer and the fragment Arg334–Gln344 is tighter, forming a visibly closer intradomain contact than in the case of the mesophilic *E. coli* ArAT structure. The small domain is slightly more compact, while the N-terminus and helix H1 are retracted into the small domain. Moreover, the other secondary-structure elements, including helices H16, H17, H18 and the i strand, are also more compact in the psychrophilic enzyme. Even though the positioning of the β-sheet is almost identical, the small differences in the helices enveloping it are visible. Helices H3, H4 and H12 are all retracted towards the β-sheet. Moreover, helices H5, H6, H7, H8, H9 and H13 are closer together, resulting in a more compact arrangement of the large domain of *Psy*ArAT than in the analogous fragment of the *E. coli* structure.

The next closest structural homologue of *Psy*ArAT is ArAT from the mesophilic bacterium *B. pseudomallei* (PDB entry 4f4e; Seattle Structural Genomics Center for Infectious Disease, unpublished work; core r.m.s.d. of aligned C$^{\alpha}$ atoms of 1.17 Å). In the N-terminal region a clear difference can be seen for the loop Asp23–Val29, which moves closer to the end of helix H16 in *Psy*ArAT compared with in *B. pseudomallei* ArAT. The distance between the tops of these superimposed loops is 2 Å. The loop Tyr36–Val45 is moved away from helix H1 in the direction of helix H14, with the distance between the residues at the top of this loop, Ser40 (*Psy*ArAT) and Asp42 (*Bur*ArAT), becoming 4.5 Å. The core of the large domain is maintained since the position of the strands and of helices H5, H6 and H7 is identical in both structures. The helices H3, H4 and H12 move towards the β-sheet core in *Psy*ArAT. Additionally, the alteration of the surface is slight, as only two short fragments of *Psy*ArAT, Asp151–Leu157 and Lys332–Arg336, move towards it. Moreover, the interactions between the two monomers of *Psy*ArAT are stronger, since the fragment Gln54–Gly72 and helix H13 move towards the second monomer.

*Psy*ArAT was compared with another ArAT from the mesophilic soil bacterium *P. denitrificans* (PDB entry 1ay4; Okamoto *et al.*, 1998), resulting in a core r.m.s.d. of 1.59 Å (Table 3). The comparison showned that the N-terminus and helix H1 are retracted inside the small domain and some of its elements, such as helices H15, H16, H17 and H18, as well as the h and i strands, are arranged closer to one another in the case of *Psy*ArAT. The large domain of *Psy*ArAT is again more compact in comparison to the *P. denitrificans* ArAT structure. Helices H5, H6, H8, H9 and H13, as well as the fragments linking H1 to H2 and H2 to H4 (including H3), are retracted to the inside of the domain in *Psy*ArAT in comparison to its mesophilic analogue. In the *Psy*ArAT structure the external helix H7 and the loop preceding it are more distant from the active site than in its mesophilic analogue. The long helix H14 of *Psy*ArAT is slightly shifted in the direction of the central β-sheet in comparison to that in the *P. denitrificans* ArAT structure (Fig. 8).

These comparisons clearly show that the compared ArATs from mesophilic bacteria are very similar to each other and display a high resemblance to the psychrophilic *Psy*ArAT. The length and distribution of the secondary-structural elements are almost identical in all of the compared structures, although some differences are visible in the positions of helices H1, H16 and H18. The structural adaptation to low temperature of the psychrophilic *Psy*ArAT is achieved not by increasing the length of the loops but by the evolutionary introduction of flexible fragments into the main peptide chain.

3.7.2. Comparison of *Psy*ArAT with ArAT from the thermophilic *P. horikoshii* OT3. A superposition of the C$^{\alpha}$ coordinates of *Psy*ArAT and those of the thermophilic bacterial ArAT from *P. horikoshii* OT3 (PDB entry 1dju; Matsui *et al.*, 2000) resulted in a core r.m.s.d. of 2.23 Å (Table 3). This comparison reveals the features that differ the

most between these two structures: the sizes of the small domain and of the core region, the interactions between the large and the small domains, and the conformation of the secondary-structure elements on the external surface of the enzymes.

Even though the thermophilic structure lacks the fragment Ala12–Lys26, a different arrangement of the N-terminus can be seen since it is placed at the intermonomer interface, while in the psychrophilic structure this segment is moved apart from the first monomer and is anchored between helices H5 and H12 of the second monomer. The fragment Asn24–Val29 in the psychrophilic structure forms a turn moved towards the small domain. Moreover, the Gly32–Cys48 fragment is longer by five amino acids, creating a loop extending outwards and shifted towards helix H16. The conformation of the peptide chain including helix H3 and the following loop Lys77–Ala96, with the one-turn helix H4 at its top, is different from that in the thermophilic enzyme, in which the analogous fragment does not contain helix H4 and is shifted in the direction of the central β-sheet. The loop Tyr149–Asp173 and helix H7 assume different conformations in the psychrophilic and thermophilic enzymes. The fragment Met210–Leu236, which includes the e strand and helix H9, is more compact, shorter by two amino acids and retracted to the core of the large domain. The top of this loop assumes a different conformation and the distance between Asp222 in *Psy*ArAT and the corresponding Asp208 in the thermophilic AT is 14.4 Å. The loop Val260–Glu269 of *Psy*ArAT is much longer than the corresponding loop (Ala247–Ser249) in its thermophilic analogue (Fig. 8). The outer surface of the large domain is expanded in the psychrophilic enzyme. The central β-sheet has a very similar conformation in both enzymes, but the helices surrounding it are slightly shifted outside. The loop Ala331–Gln344 in *Psy*ArAT with its H15 helix, which is absent in the thermophilic enzyme, is longer than the corresponding loop Glu307–Pro315 in the structure of ArAT from *P. horikoshii* OT3. Another modification that alters the outer surface of the protein is the elongation of the H5 (by three amino acids) and H12 (by five amino acids) helices and of the g strand (by three amino acids). The fragment Lys146–Leu175, which includes helix H7 and part of the c strand, is more organized and moves towards helix H8 and the surface in *Psy*ArAT. In contrast to these longer secondary-structure elements, the fragment Phe350–Pro355 is shorter in *Psy*ArAT than in the thermophilic *Pyr*ArAT by six amino acids. Similarly, the tight turn Ser371–Ser373 in the psychrophilic structure has an equivalent in the thermophilic analogue in the longer loop Pro349–Val361, which covers the entrance to the active site.

Another set of differentiating features is owing to the arrangement of the large and small domains, which come closer together in the psychrophilic aminotransferase. In *Psy*ArAT helices H3 and H6 are shifted towards the surface between the monomers in comparison to the thermophilic analogue. Moreover, the loop Pro59–Ala69 in *Psy*ArAT and the loop Ser245–Val255 are moved towards the adjacent monomer in relation to the analogous fragments in the thermophilic AT.

4. Conclusion

The crystal structure of an aminotransferase from *Psychrobacter* sp. B6 (*Psy*ArAT) described here is the first of a psychrophilic aromatic amino-acid aminotransferase. Enzymatic and structural studies of this cold-adapted aminotransferase show that it is a PLP-dependent psychrophilic enzyme with dual functionality, being specific for both aromatic amino acids and aspartate. Multiple sequence alignment shows the highest similarity to the mesophilic tyrosine aminotransferase from *E. coli* (PDB entry 3tat) and to its triple mutant (PDB entry 3fsl).

Although the adaptation of *Psy*ArAT to a psychrophilic function includes some changes in sequence similar to those observed for other psychrophilic enzymes, we did not observe the extension of the loop fragments typical of their structures. Instead, a number of glycine residues are present in the hinge fragments, leading to a higher flexibility of the enzyme over an extended temperature range. Another unique feature of this psychrophilic enzyme is its pI of 4.8, which is much lower in comparison to its mesophilic and thermophilic analogues and is a result of the presence of polar, mostly acidic, amino acids on the protein surface.

Comparison of the structure of *Psy*ArAT with bacterial ArATs, as well as with other ArATs and AspATs, leads to the conclusion that the architecture of the active centre is highly conserved among even distantly related aminotransferases.

The crystallographic studies explained which structural features are responsible for the broad substrate specificity. The arginine residues present in the active-site pocket can modulate the volume and the charge of the active site, depending on their side-chain conformation, thus allowing the accommodation of acidic and large aromatic amino acids.

The structure of the complex of *Psy*ArAT with aspartic acid obtained by cocrystallization elucidates different stages of the transamination reaction. The obtained consecutive forms of the cofactor molecule confirm the mechanism of transamination and explain the roles of particular residues in the active pocket in substrate processing. This X-ray structure confirms that the enzyme under study is not only an aromatic amino-acid aminotransferase but also an aspartate aminotransferase.

Acknowledgements

We are grateful to A. Wlodawer at NCI for his help in editing the manuscript. This work was supported by grant No. N N302 248538 from the Polish Ministry of Science and Higher Education National Science Centre (NCN). The sequence of the *psyarat* gene was deposited in GenBank with accession code GQ253123.1 and the corresponding *Psy*ArAT protein sequence was deposited in UniProt with accession code C7E5X4.

References

Altschul, S. F., Gish, W., Miller, W., Myers, E. W. & Lipman, D. J. (1990). *J. Mol. Biol.* **215**, 403–410.

Andreotti, G., Cubellis, M. W., Nitti, G., Sannia, G., Mai, X., Marino, G. & Adams, M. W. W. (1994). *Eur. J. Biochem.* **220**, 543–549.

Birolo, L., Tutino, M. L., Fontanella, B., Gerday, C., Mainolfi, K., Pascarella, S., Sannia, G., Vinci, F. & Marino, G. (2000). *Eur. J. Biochem.* **267**, 2790–2802.

Bradford, M. M. (1976). *Anal. Biochem.* **72**, 248–254.

Bujacz, G., Wrzesniewska, B. & Bujacz, A. (2010). *Acta Cryst.* D**66**, 789–796.

Chen, V. B., Arendall, W. B., Headd, J. J., Keedy, D. A., Immormino, R. M., Kapral, G. J., Murray, L. W., Richardson, J. S. & Richardson, D. C. (2010). *Acta Cryst.* D**66**, 12–21.

Dokmanić, I., Šikić, M. & Tomić, S. (2008). *Acta Cryst.* D**64**, 257–263.

Emsley, P. & Cowtan, K. (2004). *Acta Cryst.* D**60**, 2126–2132.

Feller, G. (2013). *Scientifica (Cairo)*, **2013**, 512840.

Fields, P. (2001). *Comp. Biochem. Physiol. A Mol. Integr. Physiol.* **129**, 417–431.

Gianese, G., Argos, P. & Pascarella, S. (2001). *Protein Eng. Des. Sel.* **14**, 141–148.

Grishin, N. V., Phillips, M. A. & Goldsmith, E. J. (1995). *Protein Sci.* **4**, 1291–1304.

Harding, M. M. (2006). *Acta Cryst.* D**62**, 678–682.

Hayashi, K., Inoue, H., Nagata, T., Kuramitsu, S. & Kagamiyama, H. (1993). *Biochemistry*, **32**, 12229–12239.

Hwang, B.-Y., Cho, B.-K., Yun, H., Koteshwar, K. & Kim, B.-G. (2005). *J. Mol. Catal. B Enzym.* **37**, 47–55.

Jäger, J., Moser, M., Sauder, U. & Jansonius, J. N. (1994). *J. Mol. Biol.* **239**, 285–305.

Jensen, R. A. & Gu, W. (1996). *J. Bacteriol.* **178**, 2161–2171.

Kabsch, W. (2010). *Acta Cryst.* D**66**, 125–132.

Karmen, A., Wróblewski, F. & LaDue, J. S. (1955). *J. Clin. Invest.* **34**, 131–133.

Kaufman-Szymczyk, A., Wojtasik, A., Parniewski, P., Białkowska, A., Tkaczuk, K. & Turkiewicz, M. (2009). *Acta Biochim. Pol.* **56**, 63–69.

Kirsch, J. F., Eichele, G., Ford, G. C., Vincent, M. G., Jansonius, J. N., Gehring, H. & Christen, P. (1984). *J. Mol. Biol.* **174**, 497–525.

Ko, T.-P., Wu, S.-P., Yang, W.-Z., Tsai, H. & Yuan, H. S. (1999). *Acta Cryst.* D**55**, 1474–1477.

Laemmli, U. K., Beguin, F. & Gujer-Kellenberger, G. (1970). *J. Mol. Biol.* **47**, 69–85.

Laemmli, U. K., Mölbert, E., Showe, M. & Kellenberger, E. (1970). *J. Mol. Biol.* **49**, 99–113.

Larkin, M. A., Blackshields, G., Brown, N. P., Chenna, R., McGettigan, P. A., McWilliam, H., Valentin, F., Wallace, I. M., Wilm, A., Lopez, R., Thompson, J. D., Gibson, T. J. & Higgins, D. G. (2007). *Bioinformatics*, **23**, 2947–2948.

Laskowski, R. A., MacArthur, M. W., Moss, D. S. & Thornton, J. M. (1993). *J. Appl. Cryst.* **26**, 283–291.

Lin, E. C. C., Pitt, B. M., Civen, N. & Knox, W. E. (1958). *J. Biol. Chem.* **233**, 668–673.

Maity, A. N., Chen, Y.-H. & Ke, S.-C. (2014). *Int. J. Mol. Sci.* **15**, 3064–3087.

Malashkevich, V. N., Toney, M. D. & Jansonius, J. N. (1993). *Biochemistry*, **32**, 13451–13462.

Matsui, I., Matsui, E., Sakai, Y., Kikuchi, H., Kawarabayasi, Y., Ura, H., Kawaguchi, S., Kuramitsu, S. & Harata, K. (2000). *J. Biol. Chem.* **275**, 4871–4879.

Matthews, B. W. (1968). *J. Mol. Biol.* **33**, 491–497.

McPhalen, C. A., Vincent, M. G. & Jansonius, J. N. (1992). *J. Mol. Biol.* **225**, 425–517.

Metha, P. H. & Cristen, P. (2000). *Adv. Enzymol. Relat. Areas Mol. Biol.* **74**, 129–184.

Miyahara, I., Hirotsu, K., Hayashi, H. & Kagamiyama, H. (1994). *J. Biochem.* **116**, 1001–1012.

Mueller, U., Darowski, N., Fuchs, M. R., Förster, R., Hellmig, M., Paithankar, K. S., Pühringer, S., Steffien, M., Zocher, G. & Weiss, M. S. (2012). *J. Synchrotron Rad.* **19**, 442–449.

Muratore, K. E., Engelhardt, B. E., Srouji, J. R., Jordan, M. I., Brenner, S. E. & Kirsch, J. F. (2013). *Proteins*, **81**, 1593–1609.

Murshudov, G. N., Skubák, P., Lebedev, A. A., Pannu, N. S., Steiner, R. A., Nicholls, R. A., Winn, M. D., Long, F. & Vagin, A. A. (2011). *Acta Cryst.* D**67**, 355–367.

Murshudov, G. N., Vagin, A. A. & Dodson, E. J. (1997). *Acta Cryst.* D**53**, 240–255.

Nakai, T., Okada, K., Akutsu, S., Miyahara, I., Kawaguchi, S., Kato, R., Kuramitsu, S. & Hirotsu, K. (1999). *Biochemistry*, **38**, 2413–2424.

Okamoto, A., Nakai, Y., Hayashi, H., Hirotsu, K. & Kagamiyama, H. (1998). *J. Mol. Biol.* **280**, 443–461.

Otwinowski, Z. & Minor, W. (1997). *Methods Enzymol.* **276**, 307–326.

Peña-Soler, E., Fernandez, F. J., López-Estepa, M., Garces, F., Richardson, A. J., Quintana, J. F., Rudd, K. E., Coll, M. & Vega, M. C. (2014). *PLoS One*, **9**, e102139.

Percudani, R. & Peracchi, A. (2003). *EMBO Rep.* **4**, 850–854.

Schwarzenbacher, R. *et al.* (2004). *Proteins*, **55**, 759–763.

Seetharamappa, J. *et al.* (2007). *Acta Cryst.* F**63**, 452–456.

Struvay, C. & Feller, G. (2012). *Int. J. Mol. Sci.* **13**, 11643–11665.

Taylor, P. P., Pantaleone, D. P., Senkpeil, R. F. & Fotheringham, I. G. (1998). *Trends Biotechnol.* **16**, 412–418.

Ura, H., Nakai, T., Kawaguchi, S. I., Miyahara, I., Hirotsu, K. & Kuramitsu, S. (2001). *J. Biochem.* **130**, 89–98.

Vagin, A. & Teplyakov, A. (2010). *Acta Cryst.* D**66**, 22–25.

Winn, M. D. *et al.* (2011). *Acta Cryst.* D**67**, 235–242.

Wu, H.-J., Yang, Y., Wang, S., Qiao, J.-Q., Xia, Y.-F., Wang, Y., Wang, W.-D., Gao, S.-F., Liu, J., Xue, P.-Q. & Gao, X.-W. (2011). *FEBS J.* **278**, 1345–1357.

Zheng, H., Chordia, M. D., Cooper, D. R., Chruszcz, M., Müller, P., Sheldrick, G. M. & Minor, W. (2014). *Nature Protoc.* **9**, 156–170.